Principles of cellular resource allocation revealed by condition-dependent proteome profiling

Eyal Metzl-Raz*, Moshe Kafri*, Gilad Yaakov, Ilya Soifer, Yonat Gurvich and Naama Barkai†

Department of Molecular Genetics, Weizmann Institute of Science, Rehovot 7610001, Israel.

*These authors contributed equally to this work.

†corresponding author: naama.barkai@weizmann.ac.il

Growing cells devote much of their resources to producing ribosomes. Translation of ribosomal proteins competes with the production of other proteins, suggesting that cells optimize growth by producing the precise number of ribosomes required for meeting translation demands. Alternatively, maintaining a pool of ready-to-use ribosomes could facilitate a response to fluctuating conditions. To examine how cells balance their ribosomal content, we used proteome profiling. Differences in ribosomal proteins levels in cells growing at different rates precisely accounted for the estimated differences in translation rates. However, in all conditions, 8% of the proteome coded for extra ribosomal proteins, produced in addition to the growth-rate dependent fraction. This pool of extra ribosomal proteins, consisting of ~20% of the expressed ribosomes in fast growing cells and the majority of ribosomes in slow-growing ones, was employed upon unexpected increase in translation demands, for example during nutrient upshift and when forcing excess protein production. Cells therefore tune their ribosome content and activity to balance the opposing requirements of rapid growth with rapid response to fluctuating conditions.

Keywords:

Budding yeast; translation; transcription; ribosomes; resource allocation; proteome

Cells grow in a wide range of environments by adjusting their gene expression, protein activities and metabolic fluxes. Fluctuating environments pose competing constraints on the cellular regulatory program as optimizing growth rate at each individual condition may compete with the ability to rapidly respond to changing conditions (Kussell and Leibler, 2005). For example, survival in extreme stress is greatly promoted in pre-adapted cells that already expressing stress genes at the time of stress exposure, but such expression has a cost in standard conditions (Lu et al., 2009). Perhaps accounting for this tradeoff, cells have evolved strategies to distinguish a subset of slow-growing cells that are better adapted to stress conditions (Balaban et al., 2004; Levy et al., 2012; Soll and Kraft, 1988; Yaakov et al., 2017), and for activating stress genes upon moderate stress that do not limit growth but anticipate more severe conditions (Gasch et al., 2000; Guan et al., 2012; Levy et al., 2011; Mitchell et al., 2009).

Rapid response to changing conditions may benefit cells not only when exposed to harsh environments, but also when conditions improve, for example: when cells growing in poor media are exposed to nutrient upshift. In this case, nutrient limitation is lifted and cells can increase their growth rate. However, potentially limiting in such situations is the availability of ribosomes. Ribosomes are the major resource consuming process in cells. Theoretical concepts developed over the past decades demonstrated that growth rate is maximized when all expressed ribosomes are fully employed in translation (Bosdriesz et al., 2015; Dekel and Alon, 2005; Kafri et al., 2016a; Keren et al., 2013; Klumpp et al., 2013; Koch, 1988; Li et al., 2014; Maaløe, 1979; Scott et al., 2014; Scott and Hwa, 2011; Scott et al., 2010; Shah et al., 2013; Vind et al., 1993). Under these conditions, ribosome content dictates growth rate: the specific growth is defined by the fraction of proteome which codes for ribosomal-associated proteins. In support

of that, multiple studies in a large number of organisms have found that slow growing cells express lower amounts of ribosomes compared to rapidly growing ones (Brauer et al., 2008; Bremer and Ehrenberg, 1995; Schaechter et al., 1958; Scott et al., 2010; Waldron and Lacroute, 1975; Warner, 1999; Zaslaver et al., 2009). Still, cells that fully utilize all expressed ribosomes in constant translation maximize their growth rate, but may be limited in non-constant environments. Indeed, maintaining a pool of free ribosomes may promote growth in fluctuating conditions (Champney, 1977; Koch, 1970; Varricchio and Monier, 1971; Waldron et al., 1977).

The allocation of translation resources between ribosomal and non-ribosomal proteins is therefore central to cell physiology. Still, the quantitative relation between ribosome content has and growth rate was not yet studied in eukaryotic cells. To this end, we applied proteome profiling to define the proteome composition of budding yeast growing in a range of conditions. First, we profiled cells growing exponentially in standard, low nitrogen and low-phosphate media. Second, we combined this data with published proteomic datasets of cells growing exponentially in media containing 12 different carbon sources (Paulo et al., 2015, 2016). Protein abundances were reproducible between methods and showed the expected induction of condition-specific proteins (Figure 1A-B, S1B). In standard media (SC), the proteome was dominated by proteins involved in translation (≈40%) and glycolysis (≈15%) (Figure 1C). The fraction of glycolytic proteins remained largely invariant between conditions, while the translation-related fraction decreased with growth rate, reaching ≈15% in slow-growing cells. This decrease was accompanied by increased abundance of condition-specific proteins, which in our dataset were mostly respiration-related (Figure 1D, S1A).

The proteome fraction coding ribosomal proteins increased linearly with growth rate, from ≈10% in the slowest growing cells to ≈30% in the rapidly growing ones (Figure 2A, Figure S2A,C).

The same quantitative scaling was observed when examining mRNA abundances (Figure 2B upper panel, Figure S2B), in which, it also accounted for inter-strain differences we previously described (Tamari et al., 2014, 2016). Therefore, during logarithmic growth, the proteome and transcriptome fractions devoted to ribosomal proteins scale linearly with growth rate, irrespective of the specifics of each nutrient.

To interpret the observed scaling relation between ribosome content and growth rate, we used the growth-law connecting the specific growth rate μ with the proteome fraction r_a encoding ribosomes that are actively translating at any given time: $\mu = \gamma r_a$. Here, γ denotes the rate of translating a ribosome (Kafri et al., 2016a; Maaløe, 1979; Scott et al., 2010). Written differently, this growth-law predicts the linear scaling we observe, with $r = \gamma^{-1} \mu + r_0$ where r is the ribosomal fraction, and $r_0 = r - r_a$, being the proteome fraction encoding ribosomes that are not actively translating at any given time. We previously estimated γ = 23-24 min^{-1} in budding yeast (Kafri et al., 2016b) and notably, our measurements $\Delta\mu/\Delta r = 21$ min^{-1} are well aligned with this value (Figure 2A-B). In bacteria, measurements based on rRNA content predicted $\Delta\mu/\Delta r = 6-10$ min^{-1}, consistent with the translation rate of the prokaryotic ribosome (Scott et al., 2010). Based on this, we conclude that the difference in ribosomal protein content between cells growing at different rates precisely accounts for the estimated increase in translation demands. Put in other words, the extra ribosomes expressed in rapidly growing cells are all added to the active fraction r_a , while the proteome fraction that encode for ribosomes that are not active at any given time, r_0, remains constant between conditions.

In the zero-growth regime, ribosomal proteins still account for r_0 ≈8% of the proteome (Figure 2A-B). This is consistent with experiments in both *E. coli* and budding yeast showing that arrested, or slow-growing cells maintain a pool of inactive ribosomes (Dai et al., 2016; van den

Elzen et al., 2014). Since r_0 remains constant between conditions, this implies that rapidly growing logarithmically cells also devote r_0 ≈8% of their proteome for producing ribosomal proteins that are not required for translation. Note that when considering the distribution of the ribosomes themselves between translating and non-translating state, a constant 8% of the proteome implies a much larger unsaturated ribosomal fraction, ranging from ~20% non-translating ribosomes in rapidly growing cells to the majority of ribosomes being non-translating in slowly growing cells. This ribosomal excess is increased further by genetic perturbations that reduce cell growth rate, such as gene deletions or transcriptional burden (Figure 2B, bottom panel, Figure S2D). We conclude that while cells tune their ribosomal protein content with growth rate, they still maintain a significant excess of free ribosomal proteins that are produced above the growth-rate dependent fraction.

Cells may use the excess of ribosomal proteins to accommodate an increase in translation demands. Entering stationary phase could represent such a scenario (Ju and Warner, 1994), as the reduced availability of nutrients requires an increased production of glycolytic enzymes (Figure S1A, right column). Indeed, examining published proteomic data (Murphy et al., 2015), we found that ribosomal protein content decreases (while metabolic enzymes increase) ≈2.5 generations (four hours) before the growth rate of the batch culture drops (Figure 3A, Figure S3C). Similarly, transcription profiling of cells growing in low phosphate showed an early decrease in ribosomal protein transcripts, which preceded by about five hours the reduction in growth rate (Figure S3A-B). Therefore, during preparation for stationary phase, cells reduce their overall ribosomal content but maintain their growth rate, suggesting that during this transient phase a larger fraction of the expressed ribosomes is employed in translation.

Translation demands increase when cells undergo nutrient upshifts. Under such conditions, nutrient limitation is lifted, and cells could resume fast growth practically immediately, provided that sufficient ribosomes are available to enable faster protein production. We examined the kinetics by which cells resume fast growth upon nutrient upshift by re-analyzing data we previously obtained. First, continuous cell cultures growing in a phosphate-limited chemostat responded to a spike of high phosphate within minutes (Figure 3B). Second, using a microfluidics system following individual cells transferred from galactose to glucose revealed that cells increase their specific growth rate from 0.36 hr^{-1} to 0.54 hr^{-1}, within minutes of the transfer (Figure 3C). Therefore, cells increase their growth rate, and thus protein production rates, within a short time frame that appears insufficient for synthesizing new ribosomes.

To directly correlate the ribosomal protein content and growth rate during nutrient upshift, we profiled the proteome of cells transferred from early stationary phase (OD_{600} ≈6) to fresh media (SC). Cells resumed growth rate of 0.55 hr^{-1} following a ≈40 minute lag time. Proteome profiling revealed that ribosome content did not change during the lag time, but began to increase only after cells attained fast growth (Figure 3D). Notably, during the initial growth phase, the excess of ribosomal proteins was dramatically reduced; In fact, to account for the observed growth rate during this initial growth phase, cells must have utilized the vast majority of ribosomes.

As an additional means for increasing translation demands during logarithmic growth, we engineered cells to constitutively produce high amounts of mCherry proteins (Kafri et al., 2016b)(Figure S2D), reaching ~25% of the total proteome in the highest burden cells. Growth rate and proteome composition of these burdened cells were measured in standard, low-phosphate, and low nitrogen media. In all three conditions, growth rate and the ribosomal fraction decreased with mCherry levels. When compared across conditions, ribosome content in

burdened cells scaled with growth rate with almost the same slope as wild-type (Figure 4A, S4A), consistent with an invariable translation elongation rate. Notably, in the zero-growth limit, ribosome content in high burden cells decreased from its wild-type value (≈8.1%) to just ≈5.5% proteome (Figure S4B). Therefore, the burdened cells employ a higher fraction of their ribosomes, leaving a smaller pool of free ribosomes.

The smaller fraction of free ribosomes available to burdened cells may explain their delayed recovery from starvation (Kafri et al., 2016b; Shachrai et al., 2010). Consistent with this, the burden-induced differences in recovery times were quantitatively explained by the associated difference in the ribosome excess; for example, the recovery time of the highest burden cells was prolonged by ≈30%, consistent with the same fractional decrease in its free ribosomes (Figure 4B; data from Kafri et al. (2016b)).

Our study suggests that cells tune not only the amount of ribosomes produced, but also the fraction of ribosomes that are actively translating. Thus, ribosome efficiency, defined as the ratio of active vs. free ribosomes, decreases linearly with growth rate, independently of the specifics of each nutrient (Figure 4C). Burdened cells express a lower fraction of free ribosomes, and are therefore more efficient than wild-type cells growing at the same rate (Figure 4C). Notably, when considering each condition, the ribosome efficiency in burden cells is the same as the efficiency of the faster growing wild-type cells, a prediction which we verified using polysomal profiling (Figure 4D).

The burdened cells maintain largely the same composition of the endogenous proteome (Figure S4C). Furthermore, their reduced growth rate precisely matched the decrease in the proteomic fraction occupied by the endogenous proteome (Figure 4E). Our data therefore suggests that the tuning of ribosome content and ribosome efficiency with growth rate depends primarily on

signaling from the environment (Levy et al., 2007; Martin et al., 2004; Zurita-Martinez and Cardenas, 2005) with growth-rate dependent feedbacks playing a minor role (Figure 4F).

In conclusion, we found that budding yeast growing in different environments quantitatively adjust their ribosome content with growth rate, independently of the specifics of each conditions. The relation of ribosome content with growth rate follows a simple, linear scaling law that is strikingly similar to that described in bacteria. The slopes of these linear scaling curves match their theoretically-predicted translation rate of the bacterial or eukaryotic ribosomes, respectively.

Further, the linear curves do not converge to zero at the zero-growth limit, suggesting an excess of non-translating ribosomes which occupies a constant fraction of the proteome (~8% in budding yeast). We found that this excess of ribosomes serves as a pool of ready-to-use ribosomes to enable rapid adaptation to sudden increasing translation demands. We propose that this strategy reflects a tradeoff between maximizing steady state growth rate while also maintaining the capacity to instantaneously respond to nutrient upshift in changing conditions.

Balaban, N.Q., Merrin, J., Chait, R., Kowalik, L., and Leibler, S. (2004). Bacterial Persistence as a Phenotypic Switch. Science (80-.). *305*.

Bosdriesz, E., Molenaar, D., Teusink, B., and Bruggeman, F.J. (2015). How fast-growing bacteria robustly tune their ribosome concentration to approximate growth-rate maximization. FEBS J. *282*, 2029–2044.

Brachmann, C.B., Davies, a, Cost, G.J., Caputo, E., Li, J., Hieter, P., and Boeke, J.D. (1998). Designer deletion strains derived from Saccharomyces cerevisiae S288C: a useful set of strains and plasmids for PCR-mediated gene disruption and other applications. Yeast *14*, 115–132.

Brauer, M.J., Huttenhower, C., Airoldi, E.M., Rosenstein, R., Matese, J.C., Gresham, D., Boer, V.M., Troyanskaya, O.G., and Botstein, D. (2008). Coordination of growth rate, cell cycle, stress response, and metabolic activity in yeast. Mol. Biol. Cell *19*, 352–367.

Bremer, H., and Ehrenberg, M. (1995). Guanosine tetraphosphate as a global regulator of bacterial RNA synthesis: a model involving RNA polymerase pausing and queuing. Biochim. Biophys. Acta (BBA)-Gene Struct. Expr. *1262*, 15–36.

Champney, W.S. (1977). Kinetics of ribosome synthesis during a nutritional shift-up inEscherichia coli K-12. MGG Mol. Gen. Genet. *152*, 259–266.

Charvin, G., Oikonomou, C., Siggia, E., and Cross, F. (2010). Origin of irreversibility of cell cycle start in budding yeast. PLoS Biol.

Dai, X., Zhu, M., Warren, M., Balakrishnan, R., Patsalo, V., Okano, H., Williamson, J.R., Fredrick, K., Wang, Y.-P., Hwa, T., et al. (2016). Reduction of translating ribosomes enables Escherichia coli to maintain elongation rates during slow growth. Nat. Microbiol. *2*, 16231.

Dekel, E., and Alon, U. (2005). Optimality and evolutionary tuning of the expression level of a protein. Nature *436*, 588–592.

van den Elzen, A.M.G., Schuller, A., Green, R., and Séraphin, B. (2014). Dom34-Hbs1 mediated dissociation of inactive 80S ribosomes promotes restart of translation after stress. EMBO J. *33*.

Gasch, A.P., Spellman, P.T., Kao, C.M., Carmel-Harel, O., Eisen, M.B., Storz, G., Botstein, D., and Brown, P.O. (2000). Genomic Expression Programs in the Response of Yeast Cells to Environmental Changes. Mol. Biol. Cell *11*, 4241–4257.

Gietz, R.D., and Woods, R.A. (2002). Transformation of yeast by lithium acetate/single-stranded carrier DNA/polyethylene glycol method. Methods Enzymol. *350*, 87–96.

Guan, Q., Haroon, S., Bravo, D.G., Will, J.L., and Gasch, A.P. (2012). Cellular Memory of Acquired Stress Resistance in Saccharomyces cerevisiae. Genetics *192*, 495–505.

Guerra-Moreno, A., Isasa, M., Bhanu, M.K., Waterman, D.P., Eapen, V. V., Gygi, S.P., and Hanna, J. (2015). Proteomic analysis identifies ribosome reduction as an effective proteotoxic stress response. J. Biol. Chem. *290*, 29695–29706.

Kafri, M., Metzl-Raz, E., Jonas, F., and Barkai, N. (2016a). Rethinking cell growth models. FEMS Yeast Res. *16*, fow081.

Kafri, M., Metzl-Raz, E., Jona, G., and Barkai, N. (2016b). The Cost of Protein Production. Cell Rep. *14*, 22–31.

Keller, A., Nesvizhskii, A.I., Kolker, E., and Aebersold, R. (2002). An explanation of the Peptide Prophet algorithm developed. Anal. Chem *74*, 5383–5392.

Kemmeren, P., Sameith, K., van de Pasch, L.A.L., Benschop, J.J., Lenstra, T.L., Margaritis, T., O'Duibhir, E., Apweiler, E., van Wageningen, S., Ko, C.W., et al. (2014). Large-Scale Genetic Perturbations Reveal Regulatory Networks and an Abundance of Gene-Specific Repressors. Cell *157*, 740–752.

Keren, L., Zackay, O., Lotan-Pompan, M., Barenholz, U., Dekel, E., Sasson, V., Aidelberg, G., Bren, A., Zeevi, D., Weinberger, A., et al. (2013). Promoters maintain their relative activity levels under different growth conditions. Mol. Syst. Biol. *9*, 701.

Klumpp, S., Scott, M., Pedersen, S., and Hwa, T. (2013). Molecular crowding limits translation and cell growth. Proc. Natl. Acad. Sci. U. S. A. *110*, 16754–16759.

Koch, A.L. (1970). Overall controls on the biosynthesis of ribosomes in growing bacteria. J. Theor. Biol. *28*, 203–231.

Koch, A.L. (1988). Why can't a cell grow infinitely fast? Can. J. Microbiol. *34*, 421–426.

Kussell, E., and Leibler, S. (2005). Phenotypic Diversity, Population Growth, and Information in Fluctuating Environments. Science (80-.). *309*.

Levy, S., Ihmels, J., Carmi, M., Weinberger, A., Friedlander, G., and Barkai, N. (2007). Strategy of transcription regulation in the budding yeast. PLoS One *2*, e250.

Levy, S., Kafri, M., Carmi, M., and Barkai, N. (2011). The competitive advantage of a dual-transporter system. Science *334*, 1408–1412.

Levy, S.F., Ziv, N., Siegal, M.L., Ko, M.S., Nakauchi, H., Takahashi, N., Elowitz, M.B., Levine, A.J., Siggia, E.D., Swain, P.S., et al. (2012). Bet Hedging in Yeast by Heterogeneous, Age-Correlated Expression of a Stress Protectant. PLoS Biol. *10*, e1001325.

Li, G.-W., Burkhardt, D., Gross, C., and Weissman, J.S. (2014). Quantifying absolute protein synthesis rates reveals principles underlying allocation of cellular resources. Cell *157*, 624–635.

Lu, C., Brauer, M.J., and Botstein, D. (2009). Slow growth induces heat-shock resistance in normal and respiratory-deficient yeast. Mol. Biol. Cell *20*, 891–903.

Maaløe, O. (1979). Regulation of the protein-synthesizing machinery—ribosomes, tRNA, factors, and so on. Biol. Regul. Dev.

Martin, D.E., Soulard, A., and Hall, M.N. (2004). TOR Regulates Ribosomal Protein Gene Expression via PKA and the Forkhead Transcription Factor FHL1. Cell *119*, 969–979.

Mitchell, A., Romano, G.H., Groisman, B., Yona, A., Dekel, E., Kupiec, M., Dahan, O., and Pilpel, Y. (2009). Adaptive prediction of environmental changes by microorganisms. Nature *460*, 220–224.

Murphy, J.P., Stepanova, E., Everley, R.A., Paulo, J.A., and Gygi, S.P. (2015). Comprehensive

Temporal Protein Dynamics during the Diauxic Shift in Saccharomyces cerevisiae. Mol. Cell. Proteomics *14*, 2454–2465.

O'Duibhir, E., Lijnzaad, P., Benschop, J.J., Lenstra, T.L., van Leenen, D., Groot Koerkamp, M.J.A., Margaritis, T., Brok, M.O., Kemmeren, P., and Holstege, F.C.P. (2014). Cell cycle population effects in perturbation studies. Mol. Syst. Biol. *10*, 732.

Paulo, J.A., O'Connell, J.D., Gaun, A., and Gygi, S.P. (2015). Proteome-wide quantitative multiplexed profiling of protein expression: carbon-source dependency in Saccharomyces cerevisiae. Mol. Biol. Cell *26*, 4063–4074.

Paulo, J.A., O'Connell, J.D., Everley, R.A., O'Brien, J., Gygi, M.A., and Gygi, S.P. (2016). Quantitative mass spectrometry-based multiplexing compares the abundance of 5000 S. cerevisiae proteins across 10 carbon sources. J. Proteomics *148*, 85–93.

Pospísek, M., and Valásek, L. (2013). Chapter Nine – Polysome Profile Analysis – Yeast. In Methods in Enzymology, pp. 173–181.

Schaechter, B.Y.M., Maaloe, O., and Kjeldgaard, N. (1958). Dependency on Medium and Temperature of Cell Size and Chemical Composition during Balanced Growth of Salmonella typhimurium.

Scott, M., and Hwa, T. (2011). Bacterial growth laws and their applications. Curr. Opin. Biotechnol. *22*, 565–559.

Scott, M., Gunderson, C.W., Mateescu, E.M., Zhang, Z., and Hwa, T. (2010). Interdependence of cell growth and gene expression: origins and consequences. Science *330*, 1099–1102.

Scott, M., Klumpp, S., Mateescu, E.M., and Hwa, T. (2014). Emergence of robust growth laws from optimal regulation of ribosome synthesis. Mol. Syst. Biol. *10*, 1–14.

Shachrai, I., Zaslaver, A., Alon, U., and Dekel, E. (2010). Cost of unneeded proteins in E. coli is reduced after several generations in exponential growth. Mol. Cell *38*, 758–767.

Shah, P., Ding, Y., Niemczyk, M., Kudla, G., and Plotkin, J.B. (2013). Rate-limiting steps in yeast protein translation. Cell *153*, 1589–1601.

Shalit, T., Elinger, D., Savidor, A., Gabashvili, A., and Levin, Y. (2015). MS1-Based Label-Free Proteomics Using a Quadrupole Orbitrap Mass Spectrometer. J. Proteome Res. *14*, 1979–1986.

Soll, D.R., and Kraft, B. (1988). A comparison of high frequency switching in the yeastCandida albicans and the slime moldDictyostelium discoideum. Dev. Genet. *9*, 615–628.

Tamari, Z., Rosin, D., Voichek, Y., and Barkai, N. (2014). Coordination of gene expression and growth-rate in natural populations of budding yeast. PLoS One *9*, e88801.

Tamari, Z., Yona, A.H., Pilpel, Y., and Barkai, N. (2016). Rapid evolutionary adaptation to growth on an "unfamiliar" carbon source. BMC Genomics *17*, 674.

Tong, A.H.Y., and Boone, C. (2007). Yeast Gene Analysis - Second Edition (Elsevier).

Varricchio, F., and Monier, R. (1971). Ribosome patterns in Escherichia coli growing at various

rates. J. Bacteriol. *108*, 105–110.

Vind, J., Sørensen, M.A., Rasmussen, M.D., and Pedersen, S. (1993). Synthesis of Proteins in Escherichia coli is Limited by the Concentration of Free Ribosomes. J. Mol. Biol. *231*, 678–688.

Voichek, Y., Bar-Ziv, R., and Barkai, N. (2016). Expression homeostasis during DNA replication. Science (80-.). *351*, 1087–1090.

Waldron, C., and Lacroute, F. (1975). Effect of growth rate on the amounts of ribosomal and transfer ribonucleic acids in yeast. J. Bacteriol. *122*, 855–865.

Waldron, C., Jund, R., and Lacroute, F. (1977). Evidence for a high proportion of inactive ribosomes in slow-growing yeast cells. Biochem. J. *168*, 409–415.

Wang, M., Weiss, M., Simonovic, M., Haertinger, G., Schrimpf, S.P., Hengartner, M.O., and von Mering, C. (2012). PaxDb, a database of protein abundance averages across all three domains of life. Mol. Cell. Proteomics *11*, 492–500.

Warner, J.R. (1999). The economics of ribosome biosynthesis in yeast. Trends Biochem. Sci. *24*, 437–440.

Yaakov, G., Lerner, D., Bentele, K., Steinberger, J., Barkai, N., Bigger, J., Maisonneuve, E., Gerdes, K., Lewis, K., Dhar, N., et al. (2017). Coupling phenotypic persistence to DNA damage increases genetic diversity in severe stress. Nat. Ecol. Evol. Publ. Online 4 January 2017; | doi10.1038/s41559-016-0016 *1*, 497–500.

Zaslaver, A., Kaplan, S., Bren, A., Jinich, A., Mayo, A.A., Dekel, E., Alon, U., and Itzkovitz, S. (2009). Invariant distribution of promoter activities in Escherichia coli. PLoS Comput. Biol. *5*, e1000545.

Zurita-Martinez, S.A., and Cardenas, M.E. (2005). Tor and cyclic AMP-protein kinase A: two parallel pathways regulating expression of genes required for cell growth. Eukaryot. Cell *4*, 63–71.

Acknowledgments:

We thank J. Paulo for sending the unpublished growth data, G. Jona for the assistance with the chemostats and our lab members for the fruitful discussions. This work was supported by the ERC and the ISF.

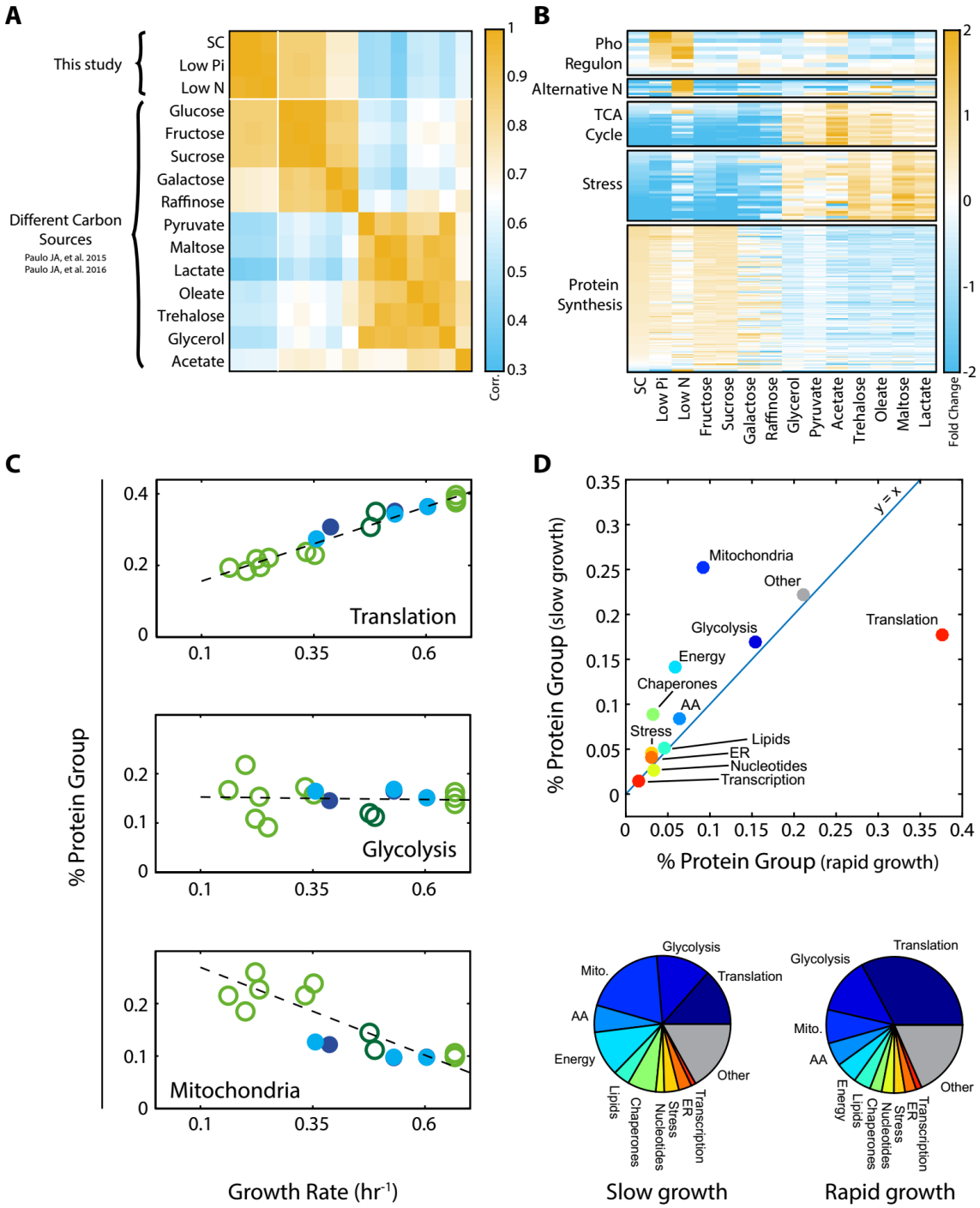

Figure 1: Proteomic analysis of budding yeast grown in different conditions:

A. *Correlation between proteome profiles of cells growing in different conditions:* Shown is the Pearson correlation between each condition to the other conditions.

B. *Condition-specific induction of specific protein groups:* Shown is the (Log_2) increase in expression relative to the median of all conditions. Proteins included in each group are specified in Table 1

C. *Mean abundance of protein groups in cells growing at different rates:* The fraction of the proteome dedicated to the specified protein group is shown as a function of cell growth rate. Filled circles correspond to data obtained in this work, empty circles are data from Paulo et al. (Paulo et al., 2015, 2016). See Figure S2A for an ordered list of conditions and Figure S1A for additional protein groups.

D. *Protein group composition in fast vs. slow growing cells:* The fraction of proteome dedicated to the indicated protein group in fast (0.63 gen/hr) or slow (0.15 gen/hr) growing cells is shown. Fast growth corresponds to standard (SC) conditions, while slow growth is extrapolated from the linear fit and includes data from all conditions as in (C) (see Figure S1A for full data). The same data is also plotted as pie-charts for a complementary presentation.

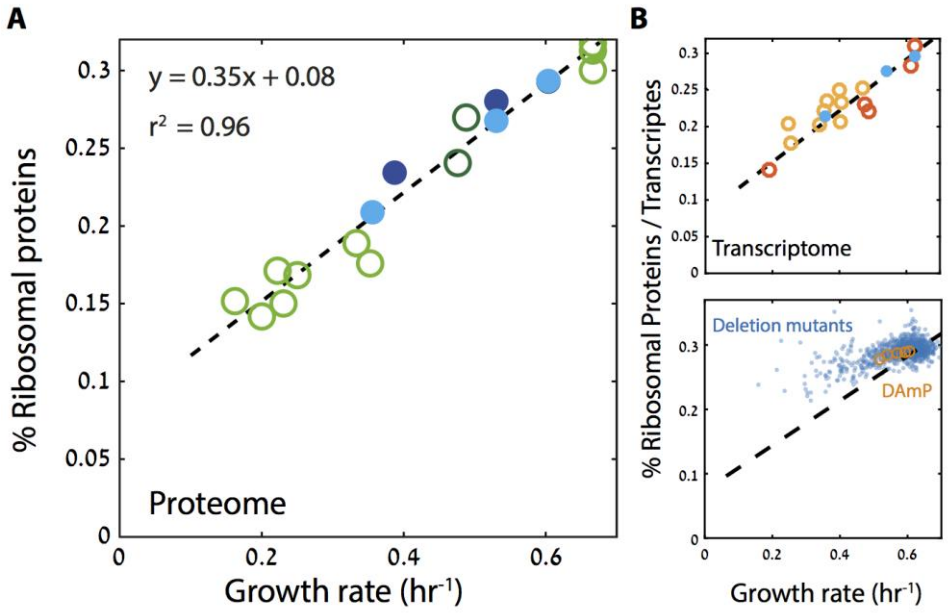

Figure 2: Ribosome content scales linearly with cell growth rate:

A. *The proteome fraction coding for ribosomal protein scales linearly with growth rate:* All proteomics data described in figure 1 were used. See Figure S2A for an ordered list of conditions. Note that the slop is 0.35x60min = 21min^{-1}

B. *Upper panel: The transcriptome fraction coding ribosomal proteins scales with growth rate:* Transcription profiles of cells growing in SC, Low Pi and Low N media were generated (filled circles). Data from previous studies describing growth in different carbon sources is also shown (open circles; data from (Gasch et al., 2000)(Orange) and (Tamari et al., 2014, 2016) (red). See Figure S2B for a full list of conditions.
Lower panel: Ribosome content in mutant cells is weakly dependent on growth rate: transcript abundances and growth rate of deletion mutants were taken from (Kemmeren et al., 2014; O'Duibhir et al., 2014) (blue filled circles). Also shown are cells forced to transcribe unstable transcripts (Kafri et al., 2016b) (DAmP, orange circles). See also figure S2D.

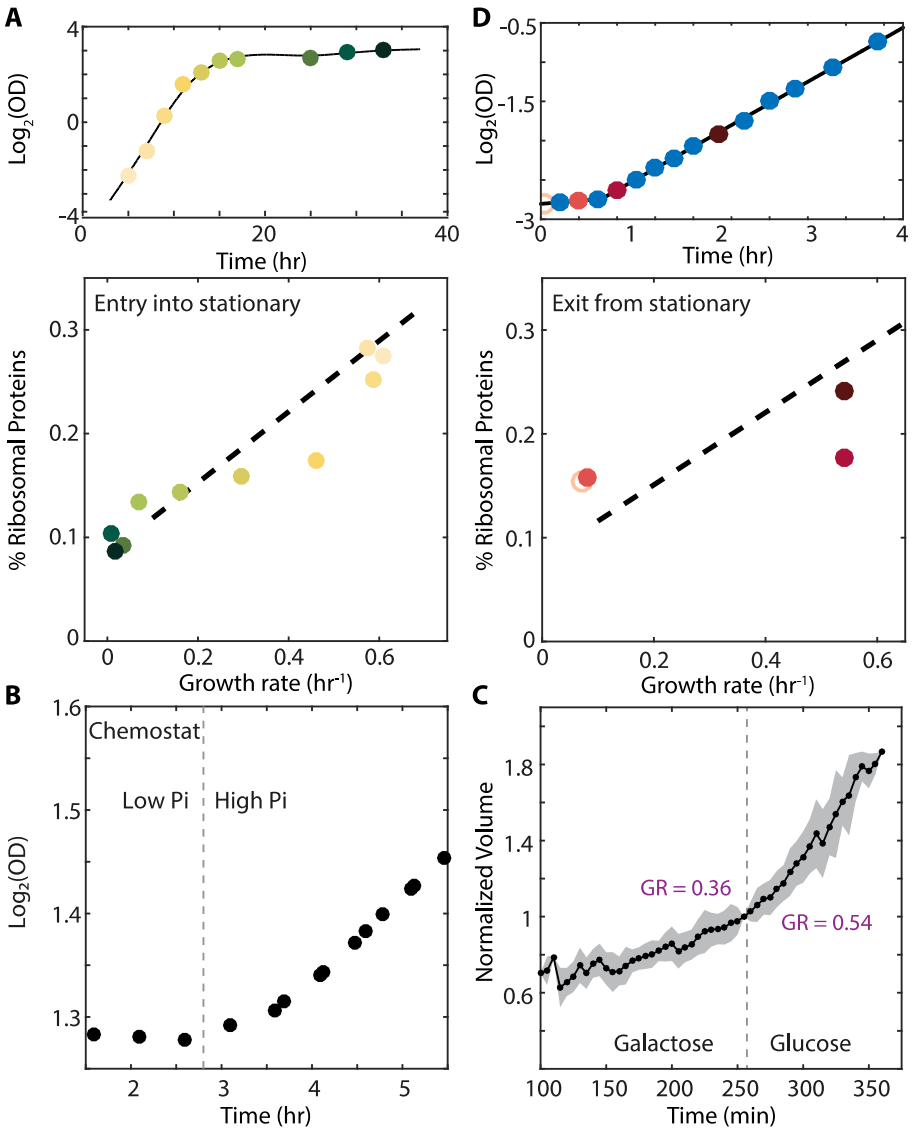

Figure 3: Cells employ the excess of ribosomal proteins in fluctuating conditions:

A. *Ribosome proteins content in batch cultures:* Shown is the ribosomal content and growth rate of cells followed along the growth curve. Data from (Murphy et al., 2015). Color gradient represents increasing time.
B. *Cells growing in phosphate-limited chemostat immediately increase their growth rate upon phosphate addition*: Continuous cultures were grown to steady state in a phosphate-limited chemostat at a dilution rate of 4.5 hr/gen. Media with high phosphate levels was injected into the growth chamber. Shown is density (OD) of the culture before and after phosphate injection.
C. *Cells resume rapid growth immediately upon transfer to a preferred carbon source:* Cells were imaged using microfluidics-coupled live-cell microscopy, as their carbon source was

changed from galactose to glucose. Shown is the average cell volume before and after the media change. Specific growth rate was calculated 25 minutes before and after the upshift.

D. *Cells existing stationary phase resume rapid growth before up-regulating their ribosome content:* Cells were grown in SC until saturation (OD_{600} ~6) and diluted back into fresh media. OD measurements were taken every 15-20 minutes as shown in the top panel, and samples for proteomic analysis were taken at the times marked in red. Color gradient represents increasing time, empty circle the initial time point. The ribosome fraction, as calculated from the proteomic data, is shown in the bottom panel. Each point is the median of three biological repeats.

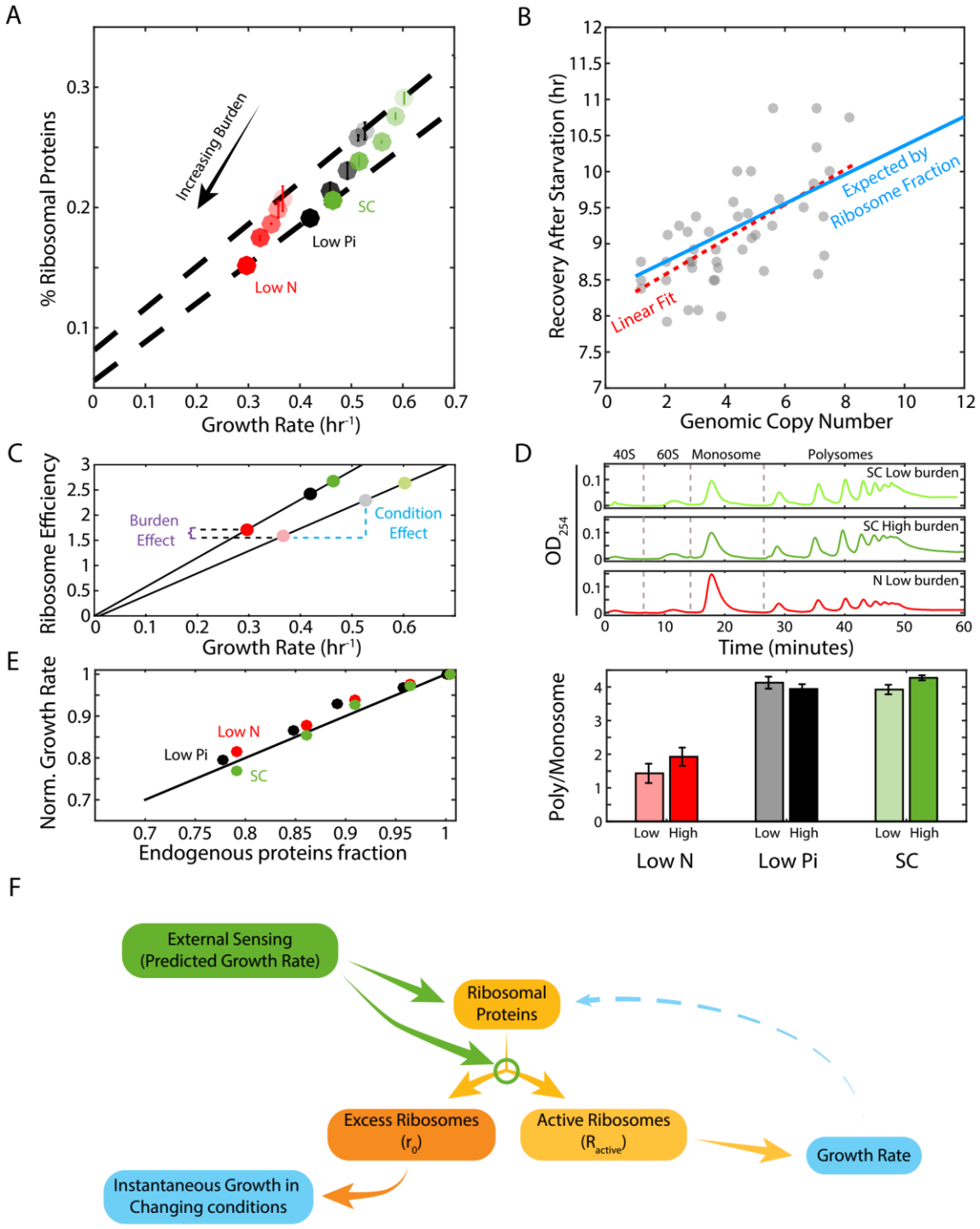

Figure 4 – Forcing unneeded proteins production reduces the pool of free ribosomes:

A. *Scaling of ribosomal protein with growth rate in burden strains:* Five strains showing increased burden were profiled in each condition. Shown is the ribosomal fraction in each strain and in each condition as a function of its growth rate.

B. *Protein burden delays recovery from starvation in proportion to its effect on the free ribosome pool*: Cells were subjected to a weeklong starvation before dilution back to standard media. Recovery times were defined when cell density increased by 50%. Dashed red line represents the expected recovery time based on the fold-reduction in free ribosomes. Data re-plotted and analyzed from (Kafri et al., 2016b).
C. *Ribosome efficiency decreases with growth rate:* We define ribosome efficiency as the ratio of active vs. free ribosomes. Shown is the ribosome efficiency as a function of growth rate in wild-type and high-burden cells. Note that for a given growth rate, ribosome efficiency in the burden cells is higher, reflecting the reduced availability of free ribosomes. However, when compared across the same conditions (same shade of color) ribosome efficiency remains invariant to the burden.
D. *The relative fraction of polysomes is invariant to protein burden:* Low and high burden cells were grown in the indicated conditions and their ribosomal content was analyzed on sucrose gradients as an indication for translational activity. Representative profiles of raw data are shown on top. The ratio between the polysomes (active transcripts with more than one ribosome bound) to detached small and large subunits (40S & 60S) together with the monosomes (mRNAs bound by a single ribosome) is shown in a bar graph on bottom. SEM error bars are based on three independent experiments.
E. *Growth rate in burdened cells follows the reduced abundance of the endogenous proteome:* The relative change in growth rate is plotted as a function of the proteome fraction occupied by the endogenous proteome (P/(P+B), where P is the total amount of endogenous proteins, and B is the amount of mCherry).
F. *Suggested Model:* Cells tune their ribosome content and ribosome efficiency based on signaling from the environment, with growth-rate dependent feedbacks playing a minor role.

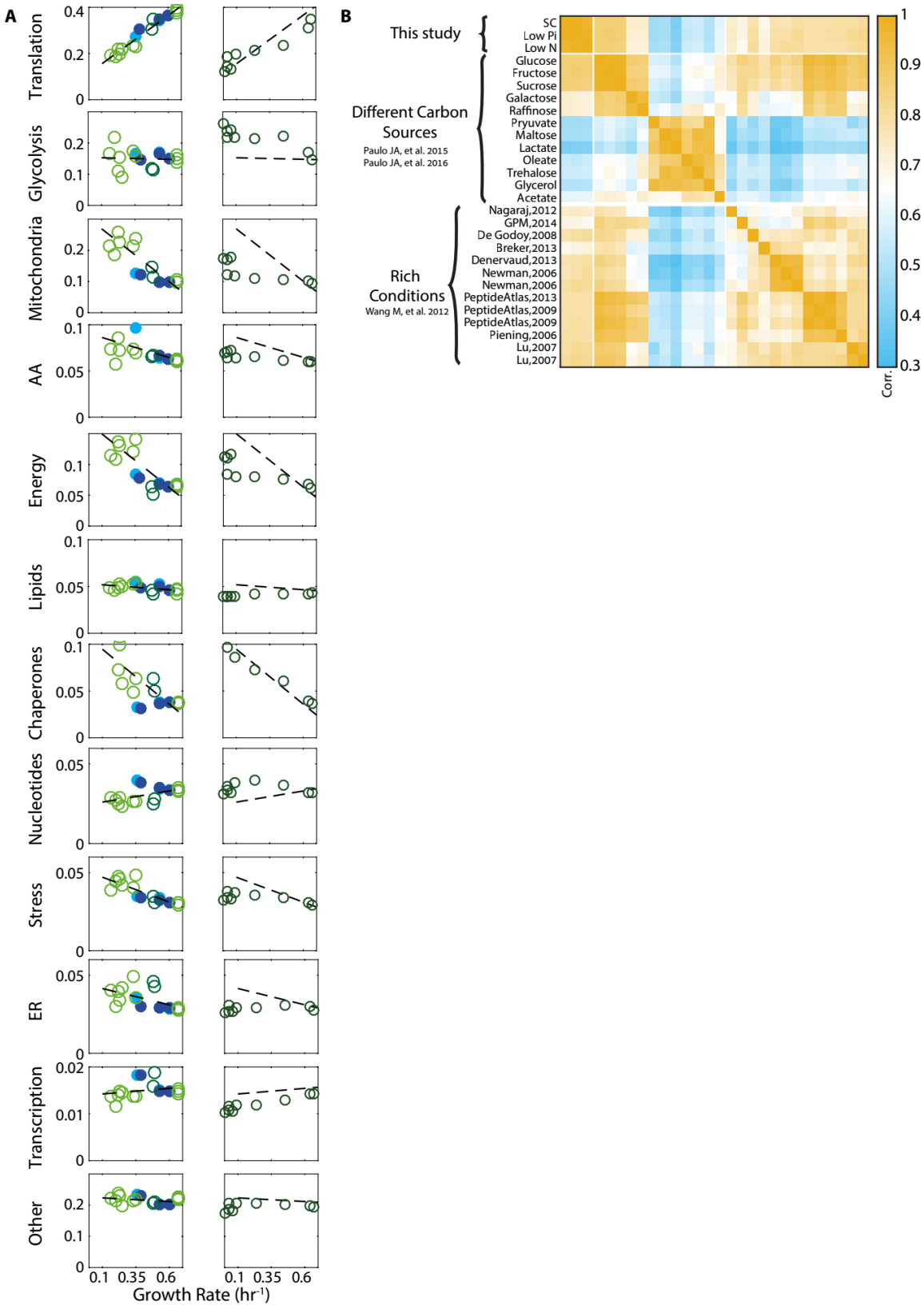

Figure S1, related to Figure 1: Proteome composition:

A. *The proteome composition under different conditions*: Left column - proteome composition of all protein groups analyzed as indicated in Figure 1C. Right column – identical protein groups, with each circle representing a time-point along the growth curve as described in Figure 3A.
B. *Correlation between proteome profiles of cells growing in different conditions:* Pearson correlation matrix as in figure 1A, including all rich condition proteomic datasets used in this study.

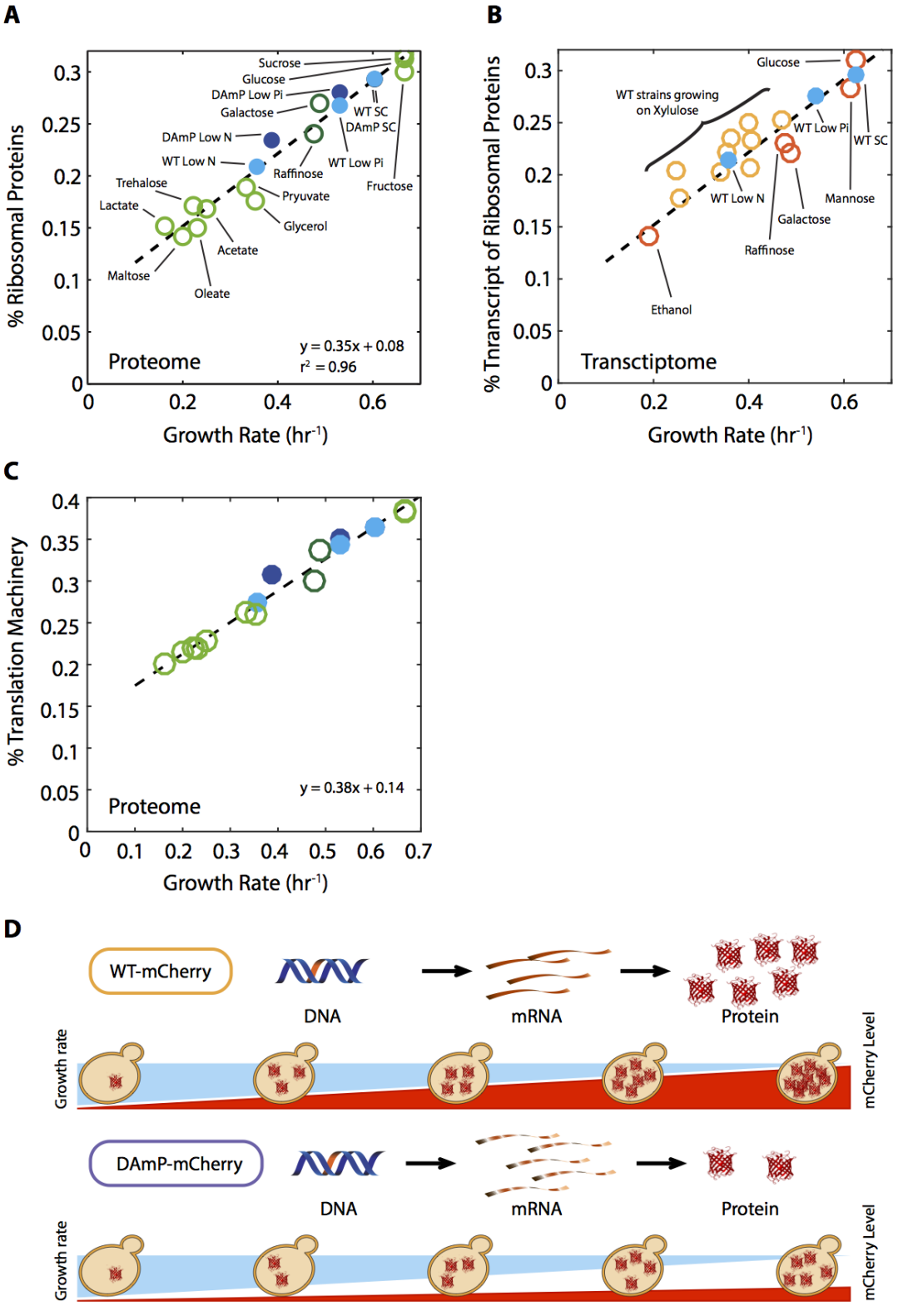

Figure S2, related to Figure 2: The proteome profiles of budding yeast cells growing in different conditions:

A. *Ribosomal fraction a function of cell growth rate:* same as figure 2A, specifying the condition.
B. Same as figure 2B, specifying the condition.
C. *Same as* (A) for a broader definition of ribosome-associated proteins, see supplemental table S1 for full list.
D. *Generation of libraries of burden cells.* See Kafri et al. (Kafri et al., 2016b).

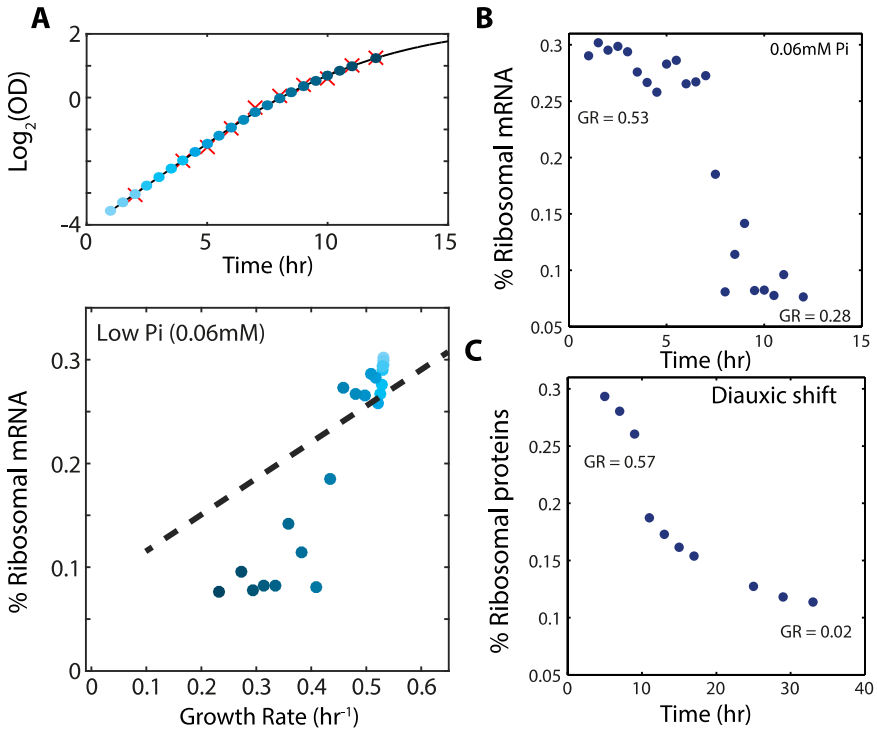

Figure S3, related to Figure 3: Cells can employ the excess ribosomes:

A. *The fraction of the transcriptome encoding ribosomal proteins in cells growing in low phosphate:* Exponentially growing cells in SC media were diluted into low phosphate media (0.06mM). OD measurements were taken every ~1/2 hour (red marks, top panel) and RNA samples were collected every ~15 minutes (blue circles, top panel). The top panel shows OD as a function of time. Color gradient representing increasing time.
B. Expression data as in (A) plotted as a function of time.
C. Proteomic data as in Figure 3A plotted as a function of time.

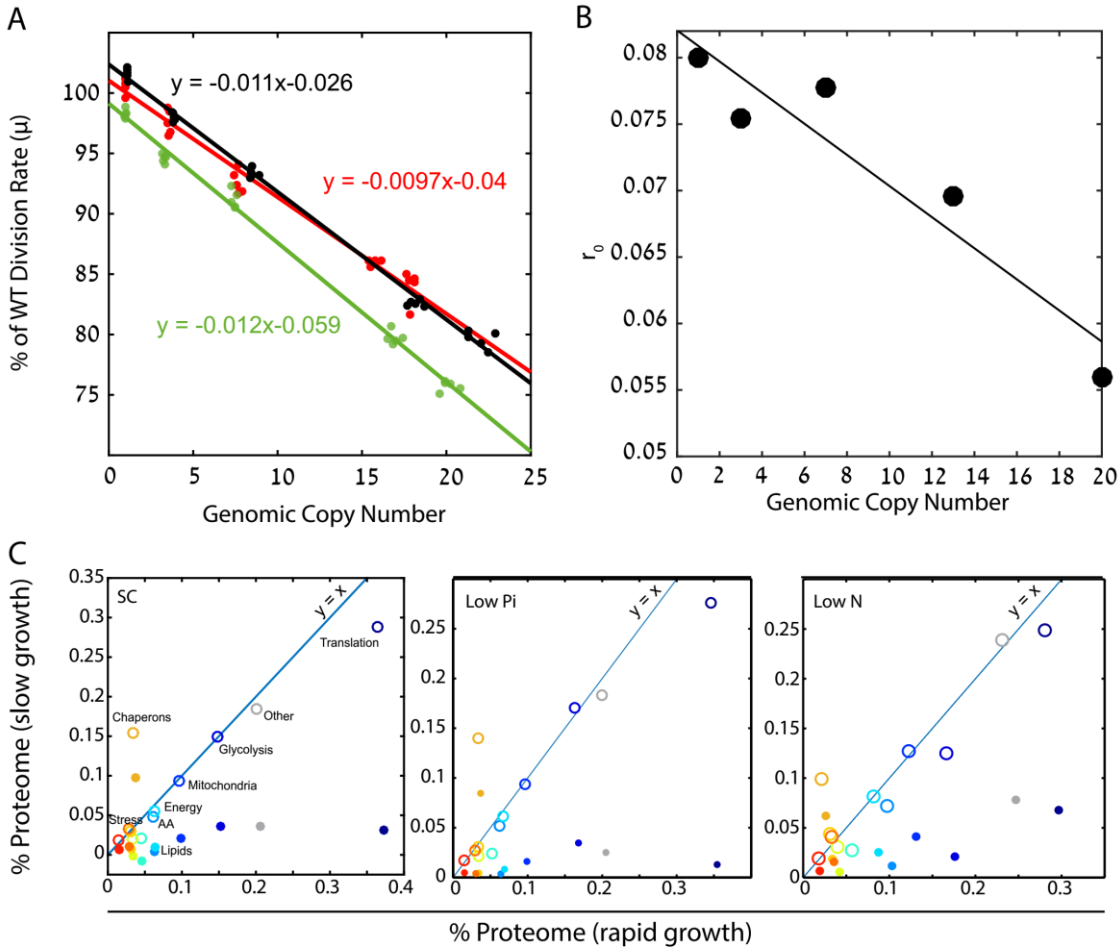

Figure S4, related to figure 4: Cells forced to produce unneeded proteins have a smaller pool of excess ribosomes:

A. *Relative growth rates of burdened cells:* The growth effect of mCherry copy number in different conditions is plotted; black low pi, green SC; red low N. Relative growth rate was calculated using competition experiments. See also (Kafri et al., 2016b).

B. *Excess ribosomes (r_0) decrease with burden*: The r_0 fraction is plotted as a function of mCherry copy number, with a linear fit in black. This fit was used for calculations that took into account r_0 of burdened cells.

C. *Burden passively impacts the ribosomal proteomic fraction:* The fraction of proteome in burdened cells dedicated to the indicated protein group in fast (one mCherry copy) or slow growing cells. Slow growth is extrapolated from the linear fit of increasing copy number. Closed circles represent all proteomic data including mCherry amounts; Open circles show only endogenous protein content.

Materials and Methods:

Media and strains

All budding yeast (*S. cerevisiae*) strains in this study were based on BY4742 (Brachmann et al., 1998) or Y8205 (Tong and Boone, 2007) laboratory strains. TDH3p-mCherry (protein fusion) was made by fusing the mCherry cassette to the end TDH3 protein using a standard PEG;LiAC;ssDNA transformation protocol (Gietz and Woods, 2002). The rest of the strains were constructed previously (Kafri et al., 2016b).
Strains were grown in SC medium or in SC medium depleted of a specific nutrient, as described in the main text. SC limiting media were prepared from YNB without the relevant nutrient (Low Phosphate medium - ForMedium, CYN0804, Low Nitrogen medium - BD 3101130). Phosphate depleted medium was prepared by adding phosphate in the form of KH_2PO_4 to a final concentration of 0.2mM. The level of potassium was preserved by adding KCl (instead of KH_2PO_4). Nitrogen limiting medium was prepared from YNB without amino acids and ammonium sulfate (BD 3101130) by adding separately 50µM of ammonium sulfate and the essential amino acids.

Strains growth rate

The stains growth rate is based mainly on the data reported previously (Kafri et al., 2016b). We validated the WT strains growth rates in the various conditions by log-phase competition assays, as described below.

Log-phase Competition

Cells were grown overnight to stationary phase in the relevant media. GFP and mCherry strains were then co-incubated in the specified media at 30˚C. The initial OD was set to ~0.05, and the WT initial frequency was ~50% of the total population. The number of generations was calculated from the dilution factor. Frequencies of GFP versus mCherry cells were measured by flow cytometry. The cells were diluted every ~8 hours. Experiments were done with WT strains expressing GFP vs. mCherry burdened cells. A linear fit of the $\log_2$ for the WT frequency dynamics was used to calculate the slope for each competition. The relative fitness advantage is calculated from the slope divided by $\log_2$. The slope of the strains' fitness advantage and their copy number were used to calculate the growth effect per copy.

Protein measurements

Sample preparation

All chemicals are from Sigma Aldrich, unless stated otherwise. Samples were subjected to in-solution tryptic digestion using a modified Filter Aided Sample Preparation protocol (FASP).

Sodium dodecyl sulfate buffer (SDT) included: 4%(w/v) SDS, 100mM Tris/HCl pH 7.6, 0.1M DTT. Urea buffer (UB): 8 M urea (Sigma, U5128) in 0.1 M Tris/HCl pH 8.0 and 50mM Ammonium Bicarbonate. Cells were dissolved in 100µL SDT buffer and lysed for 3min at 95°C. Then centrifuged at 16,000 RCF for 10min. 100ug total protein were mixed with 200 µL UB and loaded onto 30 kDa molecular weight cutoff filters and centrifuged. 200 µl of UB were added to the filter unit and centrifuged at 14,000 x g for 40 min. Alkylation using 100 µl IAA, 2 washed with Ammonium Bicarbonate. Trypsin was then added and samples incubated at 37°C overnight. Additional amount of trypsin was added and incubated for 4 hours at 37°C. Digested proteins were then spun down to a clean collecting tube, 50ul Nacl 0.5M was added and spun down, acidified with trifloroacetic acid, Desalted using HBL Oasis, Speed vac to dry and stored in -80°C until analysis.

Liquid chromatography

ULC/MS grade solvents were used for all chromatographic steps. Each sample was loaded using split-less nano-Ultra Performance Liquid Chromatography (10 kpsi nanoAcquity; Waters, Milford, MA, USA). The mobile phase was: A) H2O + 0.1% formic acid and B) acetonitrile + 0.1% formic acid. Desalting of the samples was performed online using a reversed-phase C18 trapping column (180 µm internal diameter, 20 mm length, 5 µm particle size; Waters). The peptides were then separated using a T3 HSS nano-column (75 µm internal diameter, 250 mm length, 1.8 µm particle size; Waters) at 0.35 µL/min. Peptides were eluted from the column into the mass spectrometer using the following gradient: 4% to 22%B in 145 min, 22% to 90%B in 20 min, maintained at 95% for 5 min and then back to initial conditions.

Mass Spectrometry

The nanoUPLC was coupled online through a nanoESI emitter (10 µm tip; New Objective; Woburn, MA, USA) to a quadrupole orbitrap mass spectrometer (Q Exactive Plus, Thermo Fisher Scientific, Bremen, Germany) using a FlexIon nanospray apparatus (Proxeon). Data was acquired in DDA mode, using a Top20 method. MS1 resolution was set to 70,000 (at 400m/z) and maximum injection time was set to 20msec. MS2 resolution was set to 17,500 and maximum injection time of 60msec.

Data processing and basic analysis

Raw data was imported into the Expressionist® software (Genedata) and processed as described previously (Shalit et al., 2015). The software was used for retention time alignment and peak detection of precursor peptides. A master peak list was generated from all MS/MS events and sent for database searching using Mascot v2.5 (Matrix Sciences) and MSGF+ (Integrative Omics, https://omics.pnl.gov/software/ms-gf). Data was searched against the Saccharomyces cerevisiae

(strain ATCC 204508 / S288c) protein database as downloaded from UniprotKB (http://www.uniprot.org/), and appended with 125 common laboratory contaminant proteins as well as the mCherry protein sequence (Uniprot accession X5DSL3). Fixed modification was set to carbamidomethylation of cysteines and variable modifications were set to oxidation of methionines and deamidation of N or Q. Search results were then filtered using the PeptideProphet algorithm (Keller et al., 2002) to achieve maximum false discovery rate of 1% at the protein level. Peptide identifications were imported back to Expressionist to annotate identified peaks. Quantification of proteins from the peptide data was performed using an in-house script (Keller et al., 2002). Data were normalized based on the total ion current. Protein abundance was obtained by summing the three most intense, unique peptides per protein. A Student's t-Test, after logarithmic transformation, was used to identify significant differences across the biological replica. Fold changes were calculated based on the ratio of arithmetic means of the case versus control samples.

Proteomic datasets

We analyzed the following external mass-spectrometry datasets: two carbon sources (Paulo et al., 2015, 2016), diauxic shift (Murphy et al., 2015) and arsenate data sets (Guerra-Moreno et al., 2015). In each dataset, we normalized our glucose condition or time zero to the literature (median of 13 rich conditions from PaxBD (Wang et al., 2012), see names at Figure S1B, 'Rich Conditions'). For the analysis, we used only the genes also included in our dataset. The carbon source data set (Paulo et al., 2015, 2016) growth rates were acquired from the papers or via personal communication. The diauxic shift data set (Murphy et al., 2015) growth rates were calculated from Figure 3A, upper panel by applying a growth curve to the data.

Gene groups

We divided the proteome into 12 groups, 11 groups were based mainly on SGD GO annotations or KEG annotations and together account for 80% of the proteome (by protein abundance). The rest were grouped together as an additional 12th group. There is a small overlap between the groups, See Supplementary Table 1 for the protein names in each group.

RNAseq - Protocol

As described in (Voichek et al., 2016), there are 6-8 repeats of each strain in each condition.

RNA published data sets

The different carbon data sets (Figure 2, S2) were obtained from (Gasch et al., 2000). Data on strains growing on xylulose (Figure 2B, upper panel) was obtained from (Tamari et al., 2014, 2016). We compared ribosomal fractions from the RNAseq data with ChIP data between the two

papers, and excluded from the analysis strains with high variability. Deletion strains (Figure 2B, bottom panel) datasets were obtained from (Kemmeren et al., 2014; O'Duibhir et al., 2014).

RNA data of cells growing in Low Pi media (0.06mM)

Logarithmic wild-type cells (~0.4 OD) grown in SC medium were washed in low Pi (0.06mM) media. Cells were then diluted and inoculated to fresh low Pi media; the initial OD was set to 0.05. Cells were grown in 30˚C for several hours. In every time point, as indicated at Figure S3A, a sample was extracted and RNAseq was performed as described above.

Ribosomal fraction analysis in the RNA data

The ribosomal fraction was calculated by dividing the number of RNA reads of ribosomal proteins by the total reads. In the ChIP data, the ribosomal fraction was calculated as the relative amount normalized to the SC condition (Logarithmic mean).

mCherry levels measurements

The mCherry levels were based on our mass-spectrometry data. To compare the mCherry between the different copy numbers, we used the relative mass-spectrometry date. In order to measure our reference strain (one copy in SC), we used TDH3p-mCherry (protein fusion) strain as described in the Strains section. The amount of mCherry in this strain is equal to the TDH3 protein (~2.2% base on the iBAQ parameter). The mCherry level of our one mCherry copy strain was 14.5% lower than the mCherry fluorescence of the TDH3p-mCherry strain. Thus, the mCherry level of one copy strain is ≈1.9 % of the proteome. Notably, this calibration is in very good agreement with our previous fluorescence based calibration (Kafri et al., 2016b).

Live microscopy environment perturbation experiment

Cells were grown in a standard FCS2 flow cell (Bioptechs) improved similar to (Charvin et al., 2010). Cells growing in the flow cell setup were observed with Olympus IX81 microscope with automated stage and ZDC autofocus and cooled CCD camera (Hamamatsu). In order to grow the cells in a planar layer while simultaneously control their extra cellular environment, standard FCS2 flow cell (Bioptechs) was used and improved in the following way (Charvin et al., 2010): the 40 mm round cover slips were coated with a thin layer of PDMS (Sylgrad 184, GE). This was done in a clean room, using a suitable spinning procedure to achieve layers of ~ 30 µm thick. To confine the cells and prevent their movement, while medium is flowing through the chamber (Balaban et al., 2004), a diffusive cellulose membrane, which was cut from dialysis tubes (Sigma Aldrich, D9527) was used.
The membrane was cleaned and prepared as described in (Charvin et al., 2010). The cells are

confined between the PDMS layer and the membrane, while the medium is flowing above the membrane. In this way the medium reaches the cells area without exerting too much force on the cells. The flow cell is then connected to two micro-perfusion pumps (Instech), which are controlled automatically by the computer via a D/A convener (measurement computing usb-3110), enabling to change the medium during the experiment without perturbing the cells. The media tanks for the environment perturbation experiment were continuously stirred, to allow for better aeration of the medium. The whole system is controlled by ImagePro 6.3.1 (Media Cybernetics). Cells growing in the flow cell setup were observed with Olympus IX81 microscope with automated stage and ZDC autofocus and cooled CCD camera (Hamamatsu).
Galactose to glucose shift experiments were done by replacing synthetic complete medium based on galactose (SC-Gal) with synthetic complete medium based on glucose (SC-Glu). Cell volume was estimated from the bright field images assuming that the yeast cells are prolate spheroids.

Polysome Profiling

100ml cultures of exponentially growing yeast cells (OD_{600} 0.2-0.4 with at least 6 exponential divisions since their dilution) were treated with 100µg/ml Cycloheximide for 5 minutes at 30°C, harvested, and then washed with cold Buffer AB (20mM Tris-HCl pH 7.4, 50mM KCl, 10mM MgCl2, 1mM DTT and 100µg/ml Cycloheximide). The cells were lysed with 250 ml Buffer AB using glass beads as in (Pospísek and Valásek, 2013). Cleared lysates were loaded onto 10-50% sucrose gradients with the same AB buffer composition and containing 100µg/ml Cycloheximide, and centrifuged at 39,000 RPM in a SW41 rotor for 2.5 hours at 4°C. Gradients were continuously recorded using Biocomp gradient station at OD_{254} nm. Analysis of gradients was carried out in Matlab with a customized script. Briefly, profiles were aligned in the x-axis by their peak locations and in the y-axis to SC low burden. A blank sucrose gradient measurement was subtracted from all the samples. Next, the integrals of the 40S, 60S, monosomes and polysome fractions (disomes and higher) were measured. The ratio of polysomes to monosomes was defined as the (polysomes integral) / (40S+60S+monosomes integrals).